

Precise engineering of Gemcitabine prodrug cocktails into single polymeric nanoparticles delivery for metastatic thyroid cancer cells

Chenggong Liu^{a*}, Qiongmei Han^{b*}, Hua Liu^c, Cuirong Zhu^d, Wei Gui^e, Xiaodong Yang^a and Wansen Li^a

^aDepartment of General Practice, Zhumadian City Central Hospital, Zhumadian, China; ^bDepartment of Endocrinology, Yankuang New Journey General Hospital, Jining, Shandong, China; ^cExcellent Ward, Zhumadian City Central Hospital, Zhumadian, China; ^dDepartment of Gynaecology and Obstetrics, Zhumadian Women and Children's Health Hospital, Zhumadian, China; ^eDepartment of Pharmacology Department, Zhumadian First People's Hospital, Zhumadian, China

ABSTRACT

GLOBOCAN estimates 36 types of cancers in 185 countries based on the incidence, mortality, and prevalence in the year 2019. Nowadays, chemotherapy is the most widely used cancer treatment among immune, radio, hormone, and gene therapies. Here, we describe a very simple yet cost-effective approach that synergistically combines drug reconstitution, supramolecular nano-assembly, and tumor-specific targeting to address the multiple challenges posed by the delivery of the chemotherapeutic Gemcitabine (GEM) drug. The GEM prodrugs were gifted to impulsively self-assemble into excellent steady nanoparticles size on covalent conjugation of linoleic acid hydrophobic through amide group with ~100 nm. Newly synthesized GEM-NPs morphology was confirmed by various electron microscopic techniques. After successful synthesis, we have evaluated the anticancer property of GEM and GEM-NPs against B-CPAP (papillary thyroid carcinoma) and FTC-133 (human follicular thyroid carcinoma) cancer cell lines. Further studies such as AO-EB (acridine orange-ethidium bromide), nuclear staining and flow cytometry analyses on cell death mechanism signified that the cytotoxicity was associated with apoptosis in thyroid cancer cells. GEM-NPs show excellent biocompatibility compared to GEM. The present study explained that GEM-NPs as a safe and hopeful strategy for chemotherapeutics of thyroid cancer therapy and deserve for further clinical evaluations.

ARTICLE HISTORY

Received 20 May 2020
Revised 24 June 2020
Accepted 29 June 2020

KEYWORDS



Gemcitabine prodrug; single polymeric nanoparticles; thyroid cancer; apoptosis

1. Introduction

Thyroid cancer is one of the usual endocrine malignancy cells with its occurrence steadily enhancing over the last couple of the years (Mahmoudian-Sani et al., 2019; McGonagle & Nucera, 2019; Simões-Pereira et al., 2019). Thyroid malignancy is commonly derived from stem of the thyroid follicular cells from epithelial, which can be additionally divided into the well distinguished malignancy cells, poorly discriminated malignance, and anaplastic malignance tumor cells rendering to the cancer behaviors. A distinguished thyroid malignancy cell is presently treated via thyroidectomy, succeeding radioactive iodine (RAI) treatment and long-standing thyroid triggering suppression of hormone (Bi et al., 2019; Corrigan et al., 2019; Ljubas et al., 2019; Pan et al., 2019). Although a majority of thyroid cancers have a favorable prognosis, there are scarcely any effective therapeutic approaches for metastatic thyroid cancers (Galofré et al., 2014; Kim et al., 2018; Ishihara et al., 2019; Janz et al., 2019; Wang et al., 2019). Traditional treatment strategies are usually not effective for those patients with nasty local invasion or distant metastasis, and patients harboring distant

metastasis frequently deteriorate, with a nearly 50% 5-year survival rate. In addition, if dedifferentiation occurs, thyroid cancer patients will assume more risks of neoplasm metastasis and lose RAI avidity which is always related to a poor prognosis. Since, it is urgent to search a new approach to prevent the metastasis thyroid cancer patients (Chavez et al., 2018; Garcia et al., 2019; Shelly et al., 2019; Yamazaki et al., 2019).

Gemcitabine (GEM) and its derivatives of deoxycytosine display the excellent chemotherapy available for the treatment of all types of cancer cells in the pre-clinical use. In metastasis thyroid cancer, GEM is combined to reproduce the DNA terminal chain elongations, eventually triggering the apoptosis of the tumor cells (Awasthi et al., 2012; Qin et al., 2019; Saini et al., 2020). Although these GEM analogues are applied for the therapy of thyroid patients, the treatment outcomes continue high unsatisfactory results, increasing the median of survival of thyroid patient only month (Unnam et al., 2019). The pre-clinical performance of the GEM is extensively compromised via essential obstacles including the blood flow rate of half-lifer period, quick deactivations and defecations, establishment of the drug

CONTACT Wansen Li  yxd396@163.com  Department of General Practice, Zhumadian City Central Hospital, No. 747, Zhonghua Road, Yicheng District, Zhumadian, 463000, China

*The authors contributed equally to this article.

© 2020 The Author(s). Published by Informa UK Limited, trading as Taylor & Francis Group.

This is an Open Access article distributed under the terms of the Creative Commons Attribution License (<http://creativecommons.org/licenses/by/4.0/>), which permits unrestricted use, distribution, and reproduction in any medium, provided the original work is properly cited.

resistances, and potentially serves as a side effect. Consequently, there is an essential motivation for the increased net easy but efficiency methods to completely attach GEM, which can widen the efficacy of this drug type for the managements of demoralizing the thyroid cancer (Zhang et al., 2013; Delplace et al., 2014; Kim et al., 2015; Parker et al., 2016).

Drug-delivery nanosystems capable of modulating the physicochemical properties and the *in vivo* performance of given chemotherapeutic drugs are emerging for the treatment of various diseases. Also, GEM having a hydrophilic molecules and thus incompatible with numerous polymer nanoparticles are extensively utilized in the exact biological drug delivery (De Sanctis et al., 2019; Ogunwobi & Kumar, 2019; Yajima & Akise, 2019). Hence, the biological processes to initiate the compositions with hydrophilic GEM molecules with polymeric frame works characterize the considerable challenge. This shows the problems and to enhance the stability of the nanoparticles and bioavailability of the GEM thyroid cancer treatment, by using different methods (Liu et al., 2019; Sandblom et al., 2019; Akhavan et al., 2020). Recently, GEM and its prodrugs incorporated with PEG₂₀₀₀ micelles for the excellent antitumor agents are reported by Kwon and coworkers. More recently, Cattel and research groups reported the injectable nanomedicines using GEM and its analogues show greater solubility and bioavailability (Boloix et al., 2019; Kaur et al., 2019; Oh et al., 2019). The GEM amino groups acylation did not impair the *in vitro* cytotoxic potential of small molecule prodrugs associated with lone GEM molecules (Ahn et al., 2019; Cao et al., 2019; Sibio et al., 2019; Suzuki et al., 2019; Yao et al., 2019).

In addition, after systematic managements, unpreferred adaptation of GEM to inactive uracil metabolite analogues can be substantially inhibited since decreased catabolic effects of

cytidine are abundant in the plasma membrane (Bunyatov et al., 2019; Iijima et al., 2020; Zhao et al., 2020). Therefore, the GEM encapsulation prodrug has been displayed to eliminate the drug deactivations and enhance the drug loading efficiency by misusing the improved permeability and retention effects (He et al., 2019; Thapi et al., 2019; Yan et al., 2019). In this work, we described easy and greater effect methods that actively conjugate with the drug reconstitution nano-assembly and tumor targeting agents of GEM therapies. To actively target the goal, LA is an essential fatty acid, conjugate with amino moiety of the GEM analogue through amide formation. Fruitfully, we found the GEM prodrugs increasing the self-assembly nanoparticles in the water solutions. The self-assembly GEM prodrug examined the *in vitro* cytotoxicity of thyroid cancers cells and established the morphological changes and mechanistic investigations of thyroid cancer cells.

2. Experimental section

2.1. Preparation of GEM prodrug conjugated with LA

GEM solution (50 mg, 0.19 mmol) and LA (53 mg, 0.19 mmol) having 1.5 mL of DMF was mixed into DIEA (97 mg, 7.2 mmol). The reaction mixture of the solution was allowed to stir at room temperature for overnight and then evaporated to remove DMF solution. The residue of the crude samples was immersed into the DCM. The organic layer was washed with 5% citric acid, NaCl, and aqueous NaHCO₃. Later, the DCM layer was vacuum dried with Na₂SO₄ solutions. The detailed synthetic procedures are depicted in Figure 1.

2.2. Characterization

The structure and morphology of GEM-NPs were characterized by different techniques including z-potential and

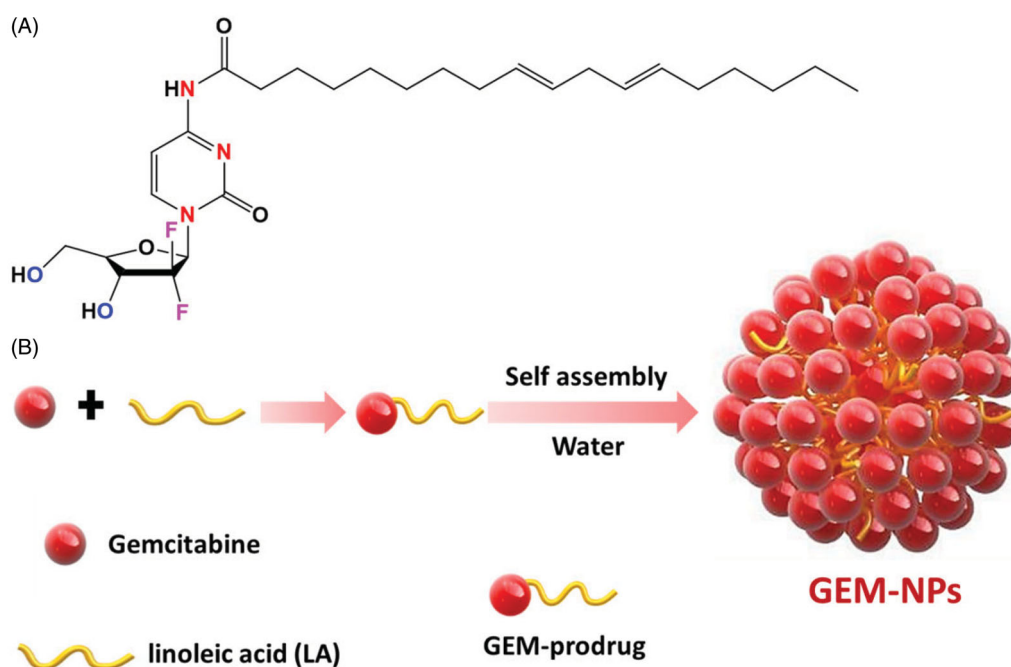


Figure 1. Schematic representation of thyroid cancer cell targeting GEM-NPs. (A) Structure of Gemcitabine (GEM). Graphic design of the preparation process of GEM prodrug formations and self-assembly of GEM-NPs in water showing potential chemotherapy effect.

dynamic light scattering (DLS). Transmission electron microscopy (TEM) and high-resolution TEM (HRTEM) were conducted on an FEI Tecnai F20 transmission electron microscope with an accelerating voltage of 200 kV.

2.3. Cell culture

Thyroid cancer cell lines B-CPAP and FTC-133 have been collected from the Department of Thoracic Surgery, the First Hospital of Jilin University, PR China. B-CPAP cells are cultured in RPMI 1640 medium (Cell Signaling, Shanghai, China) and FTC-133 cancer cells are cultured in DMEM medium complemented by 10% fetal bovine serum (Cell Signaling, Shanghai, China), penicillin and 100 µg/mL streptomycin as antibiotics (Cell Signaling, Shanghai, China) in 96-well grown which were incubated under a humid atmosphere of 5% CO₂ at 37 °C.

2.4. In vitro cytotoxicity of CCK-8 assay

A CCK-8 assay was conducted according to previously reported procedures (Akhter et al., 2020; Soni et al., 2020). It is used to determine the *in vitro* cytotoxicity of GEM and GEM-NPs. B-CPAP and FTC-133 cells were seeded into 96-well plates (4000–5000 cells in each well) and were cultured at 37 °C for 24 h. Then, the cells were subjected to constant dilution of GEM and GEM-NPs. Additionally, the result of nucleoside transporter inhibitors on the cytotoxicity of the GEM free was assessed. After incubation at 37 °C for 24 h, 10 µL of the CCK-8 solution was added to each well, and the absorbance at 520 nm was examined 2 h later by a microplate reader (Multiskan FC, Thermo Scientific, Waltham, MA). The percentage of cell inhibition by GEM and GEM-NPs was calculated and plotted in the graph by using GraphPad Prism Software (GraphPad Software, La Jolla, CA) (Ye et al., 2016; Tian et al., 2017; Cai et al., 2019). The percentage of cell viability was measured and cytotoxicity was shown as IC₅₀ and the data shown represent the average of three independent experiments. The cell viability (%) was examined using the following formula:

$$\% \text{ of cell viability} = \text{OD}_{\text{treated}} / \text{OD}_{\text{control}} \times 100$$

2.5. Cellular uptake

The cellular uptake experiments are examined according to the manufacturer's protocols. In six-well plate, 1×10^4 B-CPAP and FTC-133 thyroid cancer cell lines were imaged by LCSM (Fluoview FV 1000, Olympus, Tokyo, Japan). GEM-NP was labeled with Dil (1,1'-dioctadecyl-3,3,3',3'-tetramethylindocarbocyanine) for the examinations. In this experiment, cell lysosome was stained with LysoTracker Green DND-26 (Molecular Probe, Eugene, OR). Then, the nuclei were stained with DAPI. Subsequently, the coverslips were placed onto the glass microscope slides, and the cellular localization of GEM-NPs was pictured underneath LCSM.

2.6. In vitro drug release from the GEM and GEM-NPs

The release profiles of total GEM and GEM-NPs were monitored by dialysis using a membrane (Spectrum Laboratories, San Francisco, CA, molecular weight cut off 14 kDa). Briefly, 10 mL of GEM-NPs (0.1 mg/mL GEM or GEM-NPs equivalent concentration) were dialyzed against 20 mL of phosphate buffer solutions (PBS, pH 7.4, 0.2% Tween 80) at 37 °C. By continuous gentle stirring in an orbital shaker (100 rpm) at 37 °C, the releasing medium was collected and an equal volume of fresh medium was supplemented (You et al., 2012; Deng et al., 2015; Duo et al., 2017).

2.7. Dual (AO-EB) staining

Apoptotic morphological changes upon treatment with IC₅₀ concentration of GEM and GEM-NPs against B-CPAP and FTC-133 cancer cell lines were measured by using acridine orange and ethidium bromide (AO/EB) and Hoechst-33344 staining. After staining, the cells were visualized under a fluorescence microscope (Accu Scope EXI-310, Commack, NY) at $\times 20$ magnification (Mohamed Subarkhan et al., 2016a, 2016b, 2019; Subarkhan & Ramesh, 2016; Mohamed Kasim et al., 2018).

2.8. Flow cytometry/Annexin V-PI staining

The flow cytometry analysis with the fluorescein isothiocyanate (FITC) Annexin V Apoptosis Detection Kit (Multi Sciences, Hangzhou, China) was used to determine the B-CPAP and FTC-133 cancer cell lines apoptotic ratio. The cells were composed by trypsinization, and washed twice and resuspended in 500 µL $1 \times$ binding buffer with 5 µL of FITC Annexin V and 10 µL of PI. After 15 min, the samples were subjected to analysis by flow cytometry. The outcomes were analyzed with the BD FACS Calibur™ system (Mohan et al., 2018).

2.9. Hemolysis of GEM and GEM-NPs

Freshly collected human blood samples were collected from the Department of General Practice, Zhumadian City Central Hospital, Zhumadian 46300, China, and it was permitted by the Ethical Committee of the Department of General Practice, Zhumadian City Central Hospital, Zhumadian, China. We have conducted hemolysis according to the previously reported procedures. The blood was centrifuged and the supernatant solutions were extracted and washed with cold PBS for three times and the blood was fully eliminated and the HRBCs are obtained. Later, the HRBC solutions (0.1) were diluted with cold PBS. The solution was moved to the 5 mL tubes with 0.9 mL of DD-water added and it was used as a positive control. Further, 0.9 mL was used as a negative control. Furthermore, this PBS contains solutions of GEM and GEM-NPs (5–30 µg/mL), respectively. Later, this mixture was incubated into 3 h, continued by centrifugation and the absorbance was calculated by UV-spectrometer using the general formula. % Hemolysis = $(A_s - A_n) / (A_p - A_n) \times 100\%$, where, A_s , A_n , and A_p are the absorbances of the sample, the

negative control, and the positive control, respectively (Tramer et al., 2012; Pham et al., 2014; Chang et al., 2015).

3. Results and discussion

3.1. Synthesis and structural illustration of GEM

The GEM and GEM-NPs were prepared with some alteration in compliance with previous methods. Figure 1(B) displays the overall synthetic process. GEM analogues conjugate with various functional groups at the N-terminal ends to display the enhanced stability in the cellular plasma due to the deamination target. Further, the hydrophilic promoter of LA is utilized for the formation of amphiphilic prodrug. In this work, we designed and developed the GEM analogues to the LA functional groups to make a GEM-LA prodrug through the amide group (Figure 1). The conjugations were performed via coupling of GEM into LA under the formation of PyBOP, and the final GEM-LA prodrug was purified using TLC and column chromatographic methods with the excellent yields (75.6%). The amphiphilic nature of the prodrugs makes nanoassemblies to synthesize in the water through self-assembly methods without adding any surfactants. Additionally, the organic phases having GEM-LA prodrug was immersed in the DMSO solution into the DD-H₂O formed water suspension. More interestingly, the extra removal of the organic solvents was done via dialyzation with DD-H₂O which produced a nanosuspension rather than the prodrug precipitations. Further, the TEM examinations were performed to evaluate the morphology of the self-assembled

GEM-NPs. The outcomes of the self-assembled GEM-NPs displayed the well-organized shape with spherical structure with $\sim 79.2 \pm 9.25$ nm. Further, the hydrodynamic parameter of the self-assembled GEM-NPs was 102.5 ± 1.25 nm with less PDI, as demonstrated via DLS methods. The excellent outcomes suggested the formation of the self-assembled GEM-NPs.

3.2. In vitro GEM release from the GEM-NPs

As a typical nucleoside analogue, the major deficiencies of GEM as an anticancer drug include short half-life in plasma and rapid deactivation by cytidine deaminase. We established the self-assembly GEM-NPs could aid as pool to stably constrain the medications and obstruct medications release through general blood circulation, thus decelerating GEM authorization from the human body. The releasing profiles of GEM-NPs are examined via dialyzing against PBS at room temperature. As depicted in Figure 2(E), GEM free was quickly liberated from the GEM-NPs and plateaued at 90.2 ± 2.9 release of drug after 25 h of incubations. In contrast, GEM-NPs exhibited sustained release kinetics. Our outcomes of *in vitro* drug lease displayed the slow inhibition release kinetics of GEM free from the GEM-NPs, which is helpful for extending the blood plasma half-life of GEM free and improving the drug conveyance into tumor cells.

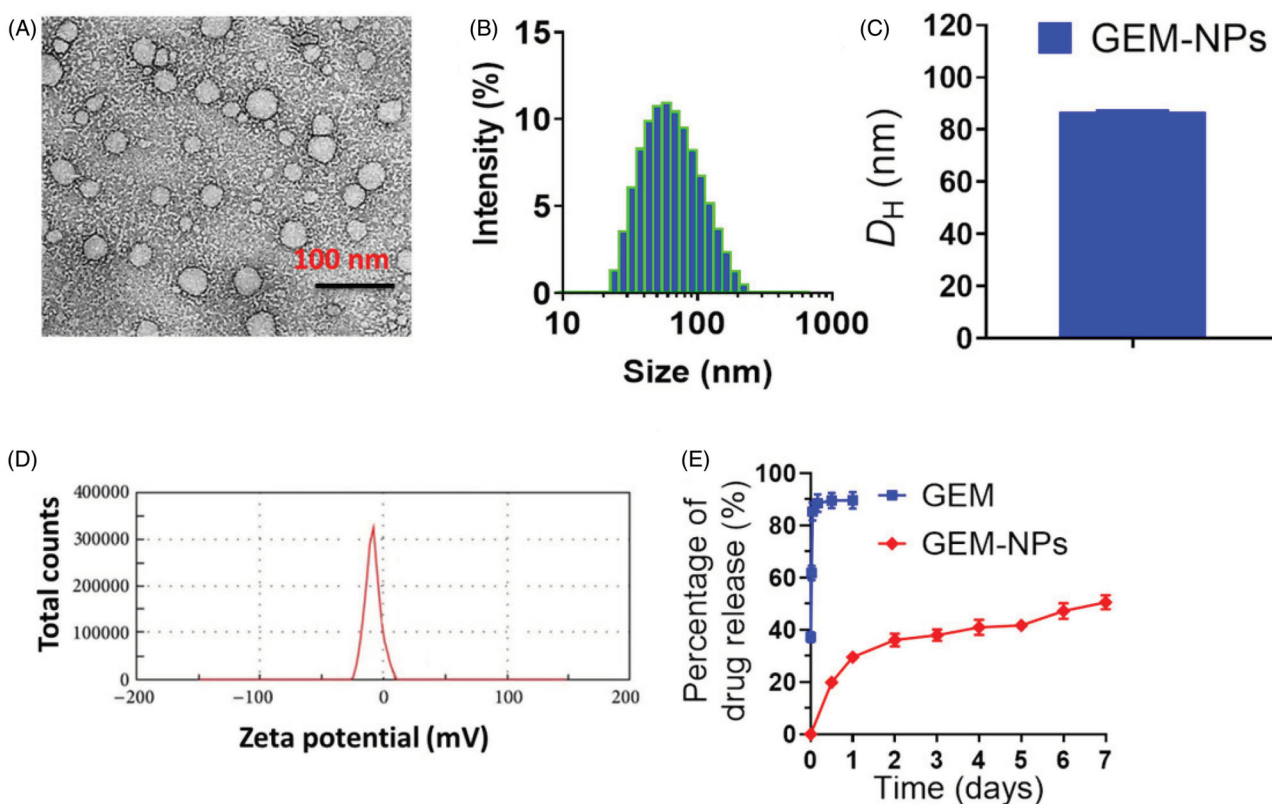


Figure 2. Characterization of GEM-NPs. (A) TEM image of GEM-NPs. Scale bar 100 nm. (B) Hydrodynamic parameter of GEM-NPs. (C) Diagram of hydrodynamic parameter of GEM-NPs. (D) Zeta potential examined via DLS analysis. (E) The solution containing GEM-NPs was dialyzed counter to PBS (pH 7.4) at 37 °C. *In vitro* drug release of GEM prodrug from GEM-NPs.

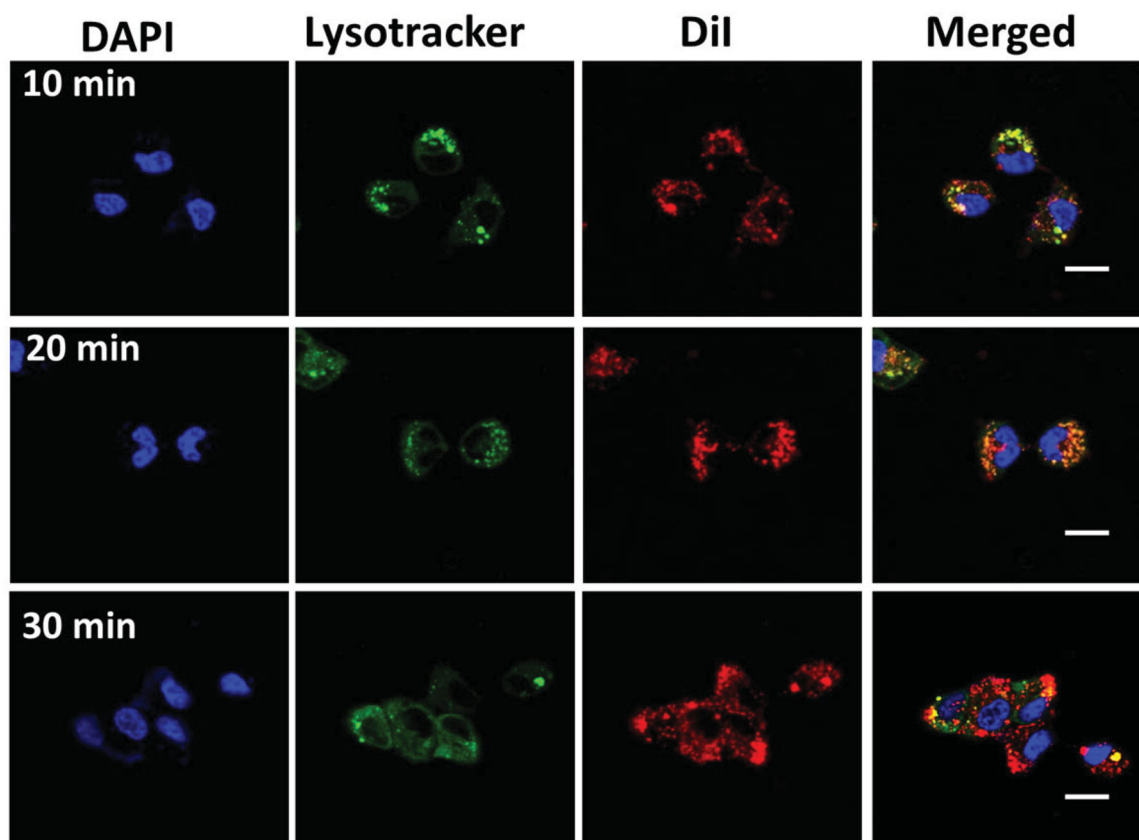


Figure 3. Subcellular localization of GEM-NPs with lysosomes in B-CPAP thyroid cancer cell lines at 10, 20, and 30 minutes incubation time. Scale bar = 20 μm .

3.3. Cellular uptake

We conjugated that the GEM-NPs enable the interface with B-CPAP and FTC-133 thyroid cancer cells and particles, hence improving the intracellular uptake into the thyroid cancer cell. To test this statement, examination of subcellular localization of GEM-NPs in the B-CPAP thyroid cancer cell lines was monitored by confocal laser scanning microscopy (CLSM) (Figure 3). The 20 nm concentrations of GEM-NPs were labeled with fluorescence marker with Dil (red color) for the investigations, on the contrast, the lysosome was stained with green LysoTracker-DND26, and the nuclei were stained with the DAPI (blue). The newly appeared yellow fluorescent was combined with LysoTracker-DND26 and Dil fluorescence in the B-CPAP thyroid cancer cell lines; therefore, GEM-NPs could be localized with lysosome after internalizations (Ahmad et al., 2020; Akhter & Amin, 2017; Akhter et al., 2018; Habban Akhter et al., 2018).

3.4. In vitro cytotoxicity

After successful synthesis of GEM-NPs, we performed the CCK-8 (cell counting kit-8) examinations to evaluate the cytotoxicity of the GEM and GEM-NPs to thyroid cancer cell lines, with B-CPAP and FTC-133 cancer cells. Next, on treatment with the medications for 24 h, the viability of the cells was monitored, and the half inhibitory concentration (IC_{50}) was obtained from the dose-dependent curve (Figure 4). Encouragingly, compared with the free drug, prodrug-assembled nanoparticles showed substantially enhanced

cytotoxic activity in both tested cell lines. For instance, in B-CPAP cell lines, the IC_{50} was 138.40 ± 11.12 and 13.62 ± 0.97 for GEM and GEM-NPs, respectively. In FTC-133 cell lines, the IC_{50} was 62.63 ± 3.30 and 25.16 ± 2.80 for GEM and GEM-NPs, respectively. Further, using free LA-GEM conjugate to test the cytotoxicity, we confirmed that PUFAylation of GEM at the 4-(N)-position indeed did not impair the potency of GEM. After entering the cells, the amide bond could be hydrolyzed by intracellular amidases such as cathepsin B or cathepsin D, thereby regenerating active GEM. GEM is a hydrophilic molecule; thus, it is difficult to diffuse through the lipid bilayer of the cell membrane. Therefore, efficient cellular uptake requires membrane nucleoside transporter proteins.

3.5. Morphological assessment

By using a fluorescent microscopic analysis of the AO-EB and Hoechst-33258 stained in B-CPAP and FTC-133 thyroid cancer cell lines, characteristic morphological changes induced by GEM and GEM-NPs were evaluated (Figure 5). The nanoparticle induces cell death via two pathways, such as apoptosis and necrosis, after treatment with their IC_{50} meditations at 24 hours. Ironically, GEM-NPs show a higher percentage of apoptotic modes of cell death than GEM free drug.

Once Hoechst-33258 staining is used, chromatin fragmentation, bi-and/or multinucleation, cytoplasmic vacuolation, nuclear swelling, cytoplasmic bleating, and late apoptosis suggestion of dot-like chromatin condensation are detected on morphological changes of thyroid cancer

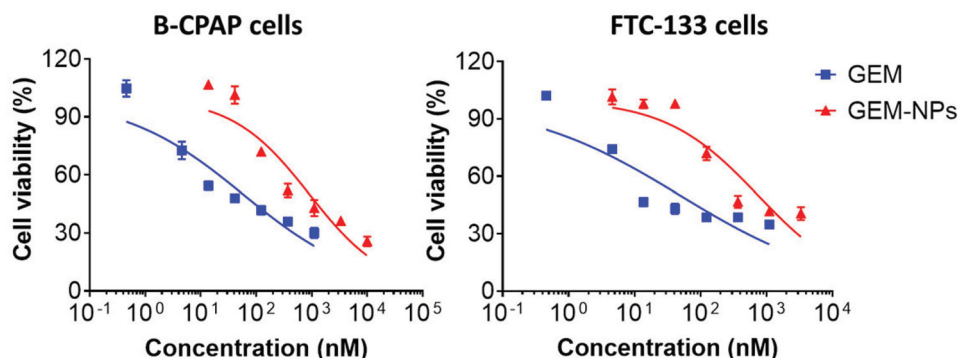


Figure 4. *In vitro* cytotoxicity of B-CPAP and FTC-133 thyroid cancer cell lines.

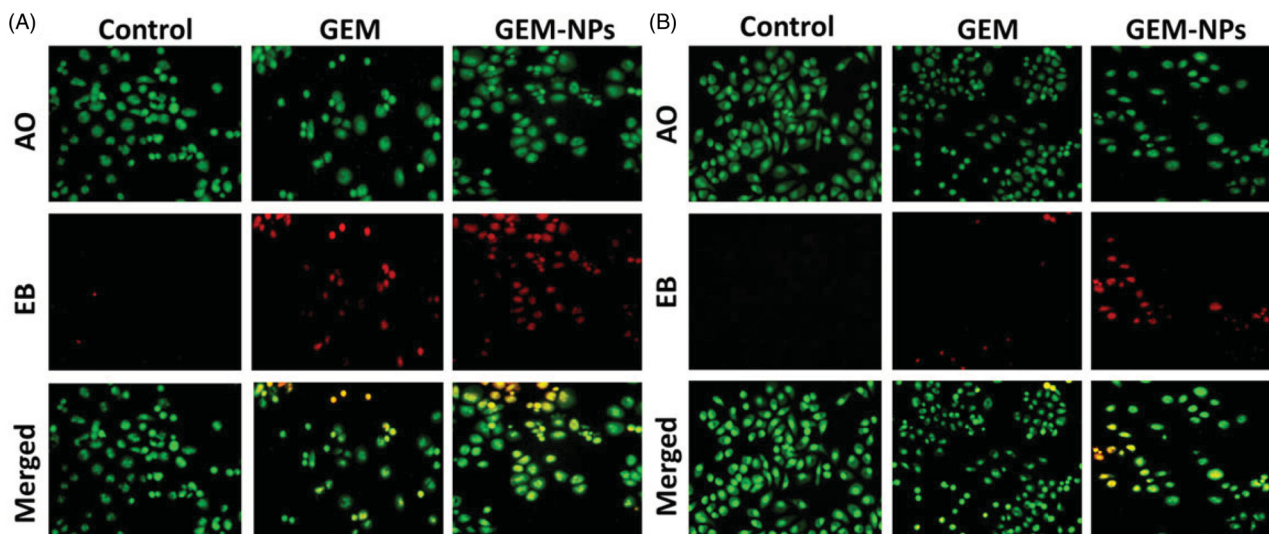


Figure 5. Dual AO/EB fluorescent staining of B-CPAP and FTC-133 thyroid cancer cell lines after treatment with GEM and GEM-NPs (IC₅₀ concentration) for 24 h.

cells. The observed cytological changes are secreted into four sorts rendering to the emission of fluorescence and the morphological characteristics of chromatin condensation in the AO-EB stained nucleus: (i) live cells with consistently green fluorescent nucleus with extreme structure; (ii) early apoptotic cells (which still have intact membranes but have begun to undergo DNA fragmentation) with green fluorescent nodes, but peri-nuclear chromatin nuclear chromatin condensation is visible as bright green patches or fragments; (iii) late apoptotic cells with orange to red fluorescent nodes with condensed or fragmented chromatin; (iv) necrotic cells swollen to huge sizes, with uniformly orange to red fluorescent nucleus with no sign of chromatin fragmentation. All these morphological modifications suggest that the thyroid cancer cells undergo apoptosis mode of cell death over the treatment of 24 hours (Figure 6). It has been stated that the anticancer action of certain GEM and GEM-NPs depends on their interaction with different proteins and their modes of binding to duplex DNA. Whole binding of plasma proteins may result in drastic alterations or even loss of the biological properties of GEM and GEM-NPs.

3.6. Apoptosis by flow cytometry

Apoptosis can be reckoned as an important impediment for a cell to become a developing cancer cell. Qualitative substantiation of apoptosis induction property of the complexes by AO-EB dual staining approach has prompted us to clarify and quantify the apoptosing cancer cells by flow cytometry using Alexa Fluor 488 Annexin V combined with propidium iodide (PI) staining assay in B-CPAP and FTC-133 thyroid cancer cell lines. Annexin V is a cell membrane impermeable protein having very high affinity toward phosphatidylserine (PS). PS is a cell cycle signaling phospholipid located inside the membrane of a healthy cell but is reverted to the outer membrane at the time of apoptosis. Hence, early and late apoptotic cells were identified as green images in the four quadrants diagram of flow cytometry by binding fluorescent conjugated Annexin V with exposed PS. PI is a DNA intercalating fluorescent dye also impermeable to the intact cell membrane but can penetrate through the damaged membrane of late apoptotic and early necrotic cells and binds to DNA fluorescent red. The cells at different stages, i.e. live cells, early apoptotic cells and late apoptotic cells were quantified in

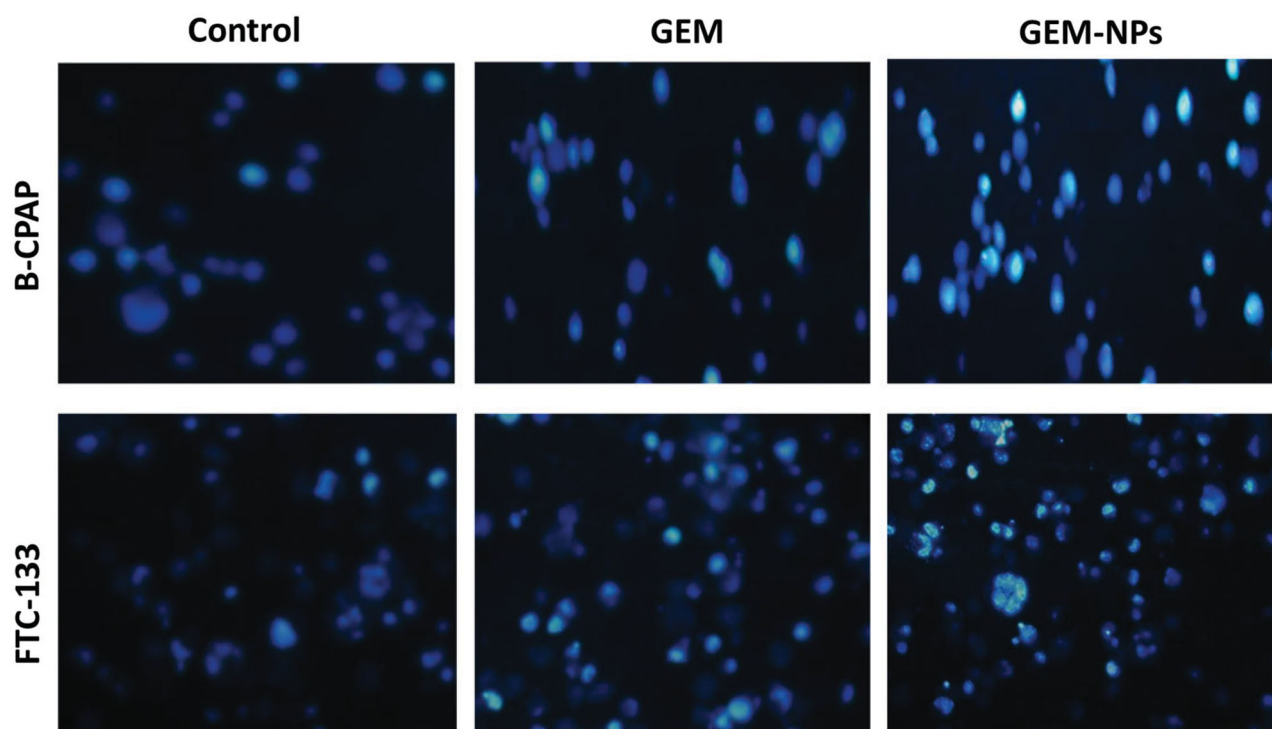


Figure 6. Nuclear staining of B-CPAP and FTC-133 thyroid cancer cell lines after treatment with GEM and GEM-NPs (IC₅₀ concentration) for 24 h.

Annexin V-/PI-, Annexin V+/PI-, and Annexin V+/PI+ quadrants respectively using fluorescence-activated cell

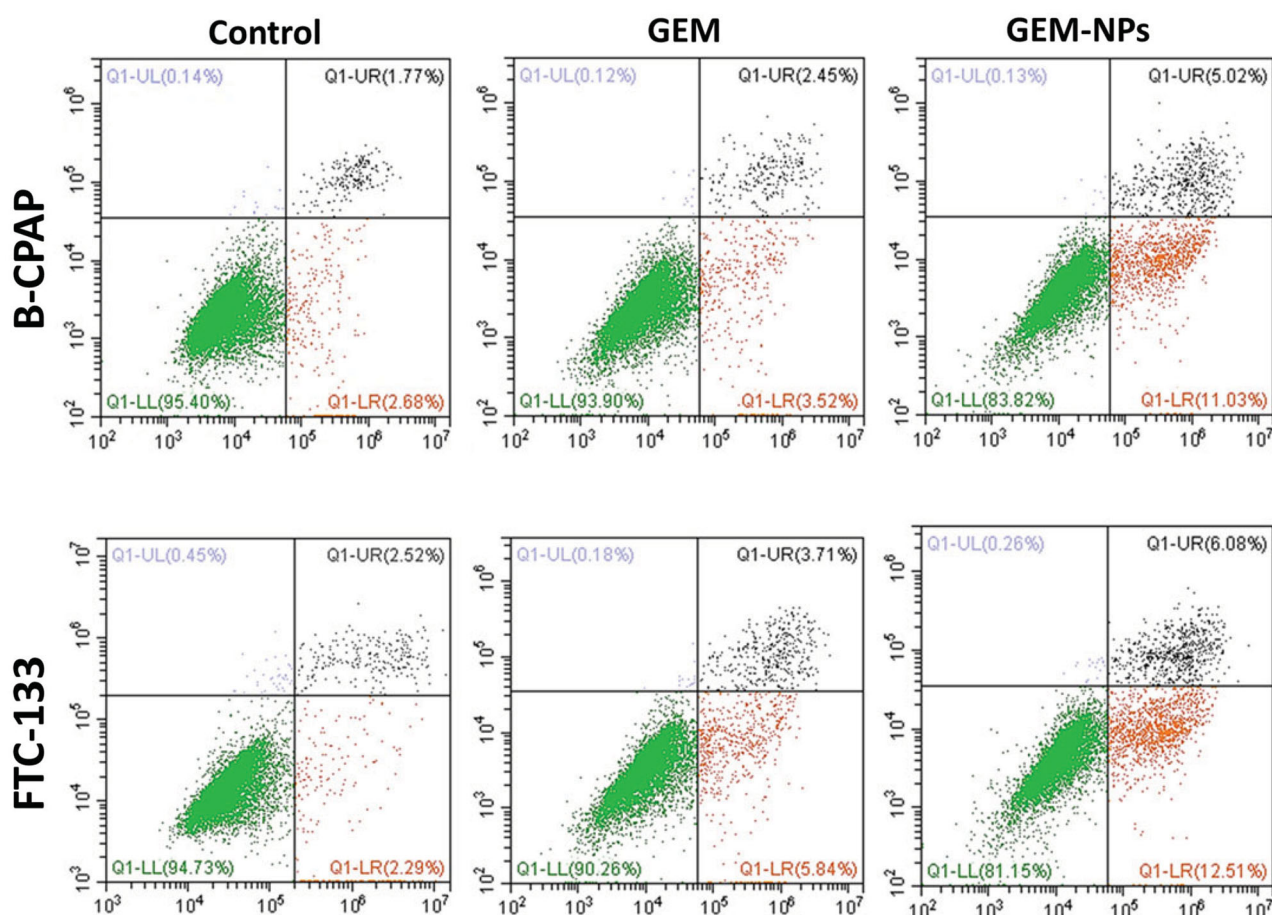


Figure 7. Apoptotic examination of B-CPAP and FTC-133 thyroid cancer cell lines using flow cytometry. The cells were treated with GEM and GEM-NPs (IC₅₀ concentration) for 24 h, and stained with FITC annexin V/PI for flow cytometry investigation.

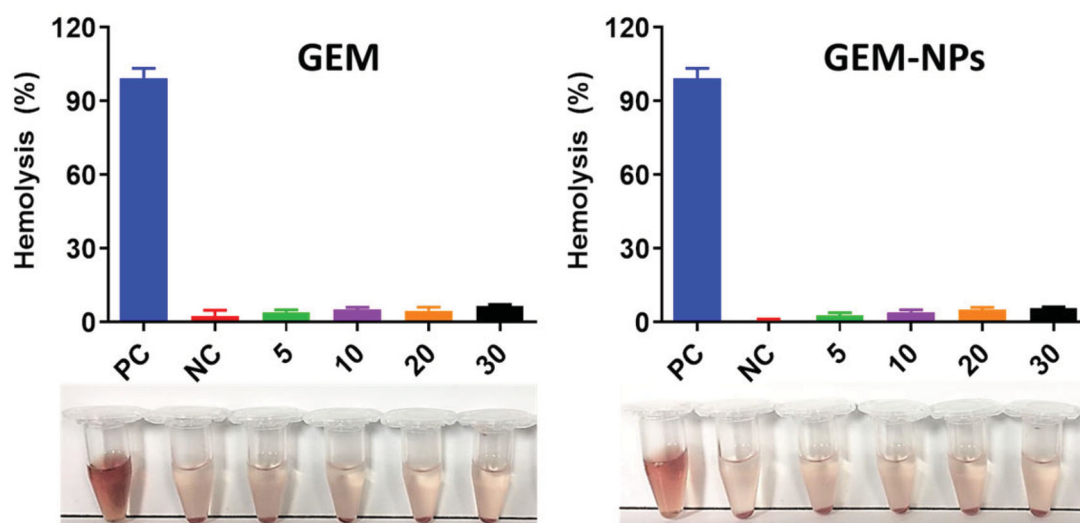


Figure 8. Hemolysis assay with different concentration of GEM and GEM-NPs. The result of hemolysis assay reveals that the insignificant hemolysis shows that it is extremely biocompatible for *in vivo* profiles.

sorting (FACS) methodology. GEM and GEM-NPs treated cancer cells exhibit different degrees of apoptosis. The late apoptotic cells are clearly indicated in Figure 7 along with the percentage of apoptotic cells. These results revealed that the complexes significantly induce apoptosis.

3.7. Hemolysis assay of GEM and GEM-NPs

The nanoformulations are predictable to interrelate with human red blood cells and cause the cell membrane damaging by hemolysis. In order to examine the human health of such adverse effects, *in vitro* biocompatibility assay was examined. The biocompatibility profiles of RBC caused by the nanoparticles were demonstrated by the different concentrations 5–30 µg/mL. Figure 8 displays the dose-dependent hemolytic effect which shows reducing toxicity of GEM and GEM-NPs. According to the results of GEM and GEM-NPs, we detected only insignificant hemolysis which shows that is extremely biocompatible for *in vivo* profiles.

4. Conclusions

In conclusion, we have successfully designed and demonstrated the hydrophilic and quick metabolized GEM prodrug to the biologically more efficient nanodrug. We point out the self-assembled GEM nanoparticles that show high DL, controlled release, and improved intracellular uptake to potentially overcome tumor cell accumulations through the effect of EPR. After positive synthesis, we have evaluated the MTT of GEM and GEM-NPs nanoparticles against B-CPAP and FTC-133 thyroid cancer cell lines. Further studies such as AO-EB (acridine orange-ethidium bromide), and flow cytometry analyses on cell death mechanism signified that the cytotoxicity was associated with apoptosis in thyroid cancer cells. Further, the morphological changes were observed using AO-EB and Hoechst-33258 staining. The results of GEM and GEM-NPs nanoparticles would invent the probable use in

thyroid patients with improved chemotherapy and future clinical investigation.

Disclosure statement

No potential conflict of interest was reported by the author(s).

References

- Ahmad J, Ameeruzzafar MZA, Akhter H. (2020). Surface-engineered cancer nanomedicine: rational design and recent progress. *Curr Pharm Des* 26:1181–90.
- Ahn J, Moyers J, Wong J, Hsueh C-T. (2019). Thyroid dysfunction from inhibitor of fibroblast growth factor receptor. *Exp Hematol Oncol* 8:6.
- Akhavan D, Yazaki P, Yamauchi D, et al. (2020). Phase I study of yttrium-90 radiolabeled M5A anti-carcinoembryonic antigen humanized antibody in patients with advanced carcinoembryonic antigen producing malignancies. *Cancer Biother Radiopharm* 35:10–15.
- Akhter MH, Amin S. (2017). An investigative approach to treatment modalities for squamous cell carcinoma of skin. *Curr Drug Deliv* 14:597–612.
- Akhter MH, Kumar S, Nomani S. (2020). Sonication tailored enhance cytotoxicity of naringenin nanoparticle in pancreatic cancer: design, optimization, and *in vitro* studies. *Drug Dev Ind Pharm* 46:659–72.
- Akhter MH, Rizwanullah M, Ahmad J, et al. (2018). Nanocarriers in advanced drug targeting: setting novel paradigm in cancer therapeutics. *Artif Cells Nanomed Biotechnol* 46:873–84.
- Awasthi N, Zhang C, Ruan W, et al. (2012). BMS-754807, a small-molecule inhibitor of insulin-like growth factor-1 receptor/insulin receptor, enhances Gemcitabine response in pancreatic cancer. *Mol Cancer Ther* 11:2644–53.
- Bi JW, Zou YL, Qian JT, Bin Chen W. (2019). MiR-599 serves a suppressive role in anaplastic thyroid cancer by activating the T-cell intracellular antigen. *Exp Ther Med* 18:2413–20.
- Boloix A, Masanas M, Jiménez C, et al. (2019). Long non-coding RNA PVT1 as a prognostic and therapeutic target in pediatric cancer. *Front Oncol* 9:1173.
- Bunyatov T, Zhao A, Kovalenko J, et al. (2019). Personalised approach in combined treatment of cholangiocarcinoma: a case report of healing from cholangiocellular carcinoma at stage IV. *J Gastrointest Oncol* 10:815–20.
- Cai L, Qin X, Xu Z, et al. (2019). Comparison of cytotoxicity evaluation of anticancer drugs between real-time cell analysis and CCK-8 method. *ACS Omega* 4:12036–42.
- Cao J, Yu Y-E, Li N-N, et al. (2019). Thyroid metastasis from non-small cell lung cancer. *Int J Clin Exp Pathol* 12:3013–21.

- Chang S-C, Liu T-P, Chen C-J, et al. (2015). Detection of heterogeneous vancomycin-intermediate *Staphylococcus aureus* isolates using a combination of δ -hemolysis assay and Etest. *Diagn Microbiol Infect Dis* 81:246–50.
- Chavez AAL, Iyer P, Cazacu IM, et al. (2018). Anaplastic thyroid carcinoma with gastric metastasis. *Curr Health Sci J* 44:294–8.
- Corrigan KL, Williamson H, Elliott Range D, et al. (2019). Treatment outcomes in anaplastic thyroid cancer. *J Thyroid Res* 2019:8218949.
- De Sanctis R, Lorenzi E, Agostinetto E, et al. (2019). Primary ovarian insufficiency associated with pazopanib therapy in a breast angiosarcoma patient: a CARE-compliant case report. *Medicine (Baltimore)* 98:e18089.
- Delplace V, Couvreur P, Nicolas J. (2014). Recent trends in the design of anticancer polymer prodrug nanocarriers. *Polym Chem* 5:1529–44.
- Deng B, Ma P, Xie Y. (2015). Reduction-sensitive polymeric nanocarriers in cancer therapy: a comprehensive review. *Nanoscale* 7:12773–95.
- Duo Y, Li Y, Chen C, et al. (2017). DOX-loaded pH-sensitive mesoporous silica nanoparticles coated with PDA and PEG induce pro-death autophagy in breast cancer. *RSC Adv* 7:39641–50.
- Galofré JC, Riesco-Eizaguirre G, Álvarez-Escolá C. (2014). Clinical guidelines for management of thyroid nodule and cancer during pregnancy. *Endocrinol Nutr (English Edition)* 61:130–8.
- García C, Buffet C, El Khattabi L, et al. (2019). MET overexpression and activation favors invasiveness in a model of anaplastic thyroid cancer. *Oncotarget* 10:2320–34.
- Habban Akhter M, Sateesh Madhav N, Ahmad J. (2018). Epidermal growth factor receptor based active targeting: a paradigm shift towards advance tumor therapy. *Artif Cells Nanomed Biotechnol* 46:1188–98.
- He R, Finan B, Mayer JP, DiMarchi RD. (2019). Peptide conjugates with small molecules designed to enhance efficacy and safety. *Molecules (Basel, Switzerland)* 24:1855.
- Iijima Y, Nakajima Y, Kinoshita H, et al. (2020). A case of resected primary pulmonary pleomorphic carcinoma with long-term survival after multidisciplinary treatment. *Surg Case Rep* 6:28.
- Ishihara S, Onoda N, Noda S, et al. (2019). Sorafenib inhibits vascular endothelial cell proliferation stimulated by anaplastic thyroid cancer cells regardless of BRAF mutation status. *Int J Oncol* 55:1069–76.
- Janz TA, Neskey DM, Nguyen SA, Lentsch EJ. (2019). Is the incidence of anaplastic thyroid cancer increasing: a population based epidemiology study. *World J Otorhinolaryngol Head Neck Surg* 5:34–40.
- Kaur S, Morris D, Ho G, et al. (2019). An unusual case of primary acinar cell carcinoma of the liver and its treatment. *J Gastrointest Oncol* 10:1021–6.
- Kim H, Kim SW, Seok KH, et al. (2018). Hypericin-assisted photodynamic therapy against anaplastic thyroid cancer. *Photodiagn Photodyn Ther* 24:15–21.
- Kim J, Pramanick S, Lee D, et al. (2015). Polymeric biomaterials for the delivery of platinum-based anticancer drugs. *Biomater Sci* 3:1002–17.
- Liu X, Li H, Wu M-L, et al. (2019). Resveratrol reverses retinoic acid resistance of anaplastic thyroid cancer cells via demethylating CRABP2 gene. *Front Endocrinol (Lausanne)* 10:734.
- Ljubas J, Ovesen T, Rusan M. (2019). A systematic review of phase II targeted therapy clinical trials in anaplastic thyroid cancer. *Cancers* 11:943.
- Mahmoudian-Sani MR, Alghasi A, Saeedi-Boroujeni A, et al. (2019). Survivin as a diagnostic and therapeutic marker for thyroid cancer. *Pathol Res Pract* 215:619–25.
- McGonagle ER, Nucera C. (2019). Clonal reconstruction of thyroid cancer: an essential strategy for preventing resistance to ultra-precision therapy. *Front Endocrinol (Lausanne)* 10:468.
- Mohamed Kasim MS, Sundar S, Rengan R. (2018). Synthesis and structure of new binuclear ruthenium(II) arene benzil bis(benzoylhydrazone) complexes: investigation on antiproliferative activity and apoptosis induction. *Inorg Chem Front* 5:585–96.
- Mohamed Subarkhan M, Prabhu RN, Raj Kumar R, Ramesh R. (2016a). Antiproliferative activity of cationic and neutral thiosemicarbazone copper(II) complexes. *RSC Adv* 6:25082–93.
- Mohamed Subarkhan MK, Ramesh R, Liu Y. (2016b). Synthesis and molecular structure of arene ruthenium(II) benzhydrazone complexes: impact of substitution at the chelating ligand and arene moiety on antiproliferative activity. *New J Chem* 40:9813–23.
- Mohamed Subarkhan MK, Ren L, Xie B, et al. (2019). Novel tetranuclear ruthenium(II) arene complexes showing potent cytotoxic and antimetastatic activity as well as low toxicity in vivo. *Eur J Med Chem* 179:246–56.
- Mohan N, Mohamed Subarkhan MK, Ramesh R. (2018). Synthesis, antiproliferative activity and apoptosis-promoting effects of arene ruthenium(II) complexes with N, O chelating ligands. *J Organomet Chem* 859:124–31.
- Ogunwobi OO, Kumar A. (2019). Chemoresistance mediated by ceRNA networks associated with the PVT1 locus. *Front Oncol* 9:834.
- Oh J, Steel M, Conklin C, Aquino-Parsons C. (2019). Metastatic gallbladder adenocarcinoma to the endometrium: a case report and review of literature. *Cureus* 11:e5258.
- Pan Z, Li L, Fang Q, et al. (2019). Integrated bioinformatics analysis of master regulators in anaplastic thyroid carcinoma. *Biomed Res Int* 2019:9734576.
- Parker JP, Ude Z, Marmion CJ. (2016). Exploiting developments in nanotechnology for the preferential delivery of platinum-based anti-cancer agents to tumours: targeting some of the hallmarks of cancer. *Metalomics* 8:43–60.
- Pham CTN, Thomas DG, Beiser J, et al. (2014). Application of a hemolysis assay for analysis of complement activation by perfluorocarbon nanoparticles. *Nanomedicine* 10:651–60.
- Qin L, Ling G, Peng F, et al. (2019). Black phosphorus nanosheets and Gemcitabine encapsulated thermo-sensitive hydrogel for synergistic photothermal-chemotherapy. *J Colloid Interface Sci* 556:232–8.
- Saini K, Prabhuraj RS, Bandyopadhyaya R. (2020). Development of mesoporous silica nanoparticles of tunable pore diameter for superior Gemcitabine drug delivery in pancreatic cancer cells. *J Nanosci Nanotechnol* 20:3084–96.
- Sandblom V, Spetz J, Shubbar E, et al. (2019). Gemcitabine potentiates the anti-tumour effect of radiation on medullary thyroid cancer. *PLoS One* 14:e0225260.
- Shelly D, Gupta D, Mishra S, Bharadwaj R. (2019). Osteoclastic variant of anaplastic thyroid carcinoma: a case report of rare entity. *J Cancer Res Ther* 15:704–7.
- Sibio S, Sica GS, Carlo SD, et al. (2019). Surgical treatment of intraperitoneal metastases from lung cancer: two case reports and a review of the literature. *J Med Case Rep* 13:262.
- Simões-Pereira J, Capitão R, Lambert E, Leite V. (2019). Anaplastic thyroid cancer: clinical picture of the last two decades at a single oncology referral centre and novel therapeutic options. *Cancers* 11:1188.
- Soni K, Mujtaba A, Akhter MH, et al. (2020). Optimisation of ethosomal nanogel for topical nano-CUR and sulphoraphane delivery in effective skin cancer therapy. *J Microencapsul* 37:91–108.
- Subarkhan MKM, Ramesh R. (2016). Ruthenium(II) arene complexes containing benzhydrazone ligands: synthesis, structure and antiproliferative activity. *Inorg Chem Front* 3:1245–55.
- Suzuki Y, Imasato M, Nakahara Y, et al. (2019). Metachronous rectal metastasis from pulmonary adenocarcinoma after 11 years of chemo-, immuno-, and radiotherapy for recurrent lesions: a case report. *Surg Case Rep* 5:151.
- Thapi S, Leiter A, Galsky M, Gallagher EJ. (2019). Recovery from secondary adrenal insufficiency in a patient with immune checkpoint inhibitor therapy induced hypophysitis. *J Immunother Cancer* 7:248.
- Tian F, Ling Y, Chen Y, Wang Z. (2017). Effects of CCK-8 and cystathionine γ -lyase/hydrogen sulfide system on acute lung injury in rats. *Inflammation* 40:174–83.
- Tramer F, Da Ros T, Passamonti S. (2012). Screening of fullerene toxicity by hemolysis assay. *Methods Mol Biol* 926:203–17.

- Unnam S, Panduragaiah VM, Sidramappa MA, Muddana Eswara BR. (2019). Gemcitabine-loaded folic acid tagged liposomes: improved pharmacokinetic and biodistribution profile. *Curr Drug Deliv* 16: 111–22.
- Wang JR, Zafereo ME, Dadu R, et al. (2019). Complete surgical resection following neoadjuvant dabrafenib plus trametinib in BRAFV600E-mutated anaplastic thyroid carcinoma. *Thyroid* 29:1036–43.
- Yajima K, Akise Y. (2019). A case report of Graves' disease induced by the anti-human programmed cell death-1 monoclonal antibody pembrolizumab in a bladder cancer patient. *Case Rep Endocrinol* 2019: 2314032.
- Yamazaki H, Iwasaki H, Suganuma N, et al. (2019). Anaplastic thyroid carcinoma diagnosed after treatment of lenvatinib for papillary thyroid carcinoma. *Endocrinol Diabetes Metab Case Rep*.
- Yan P, Su Z, Zhang Z, Gao T. (2019). LncRNA NEAT1 enhances the resistance of anaplastic thyroid carcinoma cells to cisplatin by sponging miR-9-5p and regulating SPAG9 expression. *Int J Oncol* 55: 988–1002.
- Yao N, Chen Q, Shi W, et al. (2019). PARP14 promotes the proliferation and Gemcitabine chemoresistance of pancreatic cancer cells through activation of NF- κ B pathway. *Mol Carcinog* 58: 1291–302.
- Ye G, Tao L, Ma C, et al. (2016). Influences of CCK-8 on expressions of apoptosis-related genes in prefrontal cortex neurons of morphine-relapse rats. *Neurosci Lett* 631:115–21.
- You J, Zhang R, Xiong C, et al. (2012). Effective photothermal chemotherapy using doxorubicin-loaded gold nanospheres that target EphB4 receptors in tumors. *Cancer Res* 72:4777–86.
- Zhang Y, Kim WY, Huang L. (2013). Systemic delivery of Gemcitabine triphosphate via LCP nanoparticles for NSCLC and pancreatic cancer therapy. *Biomaterials* 34:3447–58.
- Zhao D, Jiang M, Zhang X, Hou H. (2020). The role of RICTOR amplification in targeted therapy and drug resistance. *Mol Med* 26:20.